Featured Article

Characterization of Gastrin-Induced Proangiogenic Effects *In vivo* in Orthotopic U373 Experimental Human Glioblastomas and *In vitro* in Human Umbilical Vein Endothelial Cells

Florence Lefranc,[1] Tatjana Mijatovic,[3] Véronique Mathieu,[3] Sandrine Rorive,[2] Christine Decaestecker,[3] Olivier Debeir,[4] Jacques Brotchi,[1] Philippe Van Ham,[4] Isabelle Salmon,[2] and Robert Kiss[3]

[1]Department of Neurosurgery and [2]Laboratory of Pathology, Erasmus University Hospital; [3]Laboratory of Toxicology, Institute of Pharmacy; and [4]Department of Logical and Numerical Systems, Faculty of Applied Sciences, Université Libre de Bruxelles, Brussels, Belgium

ABSTRACT

Purpose: **This study aims to investigate the role of gastrin-17 (G17) on angiogenesis features in gliomas both *in vitro* and *in vivo*.**

Experimental Design: **The influences of G17 and G17 receptor antagonists were characterized *in vitro* in terms of angiogenesis on human umbilical vein endothelial cell (HUVEC) tubulogenesis processes on Matrigel and *in vivo* with respect to U373 orthotopic glioma xenografts. The influence of phosphatidylinositol 3′-kinase, protein kinase C, and nuclear factor-κB inhibitors was characterized *in vitro* on G17-mediated HUVEC tubulogenesis. G17-mediated release of interleukin (IL)-8 from HUVECs and G17-induced modifications in nuclear factor-κB DNA binding activity were characterized by means of specific enzyme-linked immunosorbent assays. The influence of G17 on E- and P-selectin expression was determined by means of computer-assisted microscopy, whereas the influence of E- and P-selectin on HUVEC migration was approached by means of antisense oligonucleotides. The chemotactic influence of G17 and IL-8 on HUVEC migration was characterized by means of computer-assisted videomicroscopy with Dunn chambers.**

Results: **Messenger RNAs for cholecystokinin $(CCK)_A$, CCK_B, and CCK_C receptors were present in HUVECs and microvessels dissected from a human glioblastoma. Whereas G17 significantly increased the levels of angiogenesis *in vivo* in the U373 experimental glioma model and *in vitro* in the HUVECs, the CCK_B receptor antagonist L365,260 significantly counteracted the G17-mediated proangiogenic effects. G17 chemoattracted HUVECs, whereas IL-8 failed to do so. IL-8 receptor α (CXCR1) and IL-8 receptor β (CXCR2) mRNAs were not detected in these endothelial cells. Gastrin significantly (but only transiently) decreased the level of expression of E-selectin, but not P-selectin, whereas IL-8 increased the expression of E-selectin. Specific antisense oligonucleotides against E- and P-selectin significantly decreased HUVEC tubulogenesis processes *in vitro* on Matrigel.**

Conclusions: **The present study shows that gastrin has marked proangiogenic effects *in vivo* on experimental gliomas and *in vitro* on HUVECs. This effect depends in part on the level of E-selectin activation, but not on IL-8 expression/release by HUVECs.**

INTRODUCTION

Glioblastoma multiforme (GBM) is the most malignant and most common variant of human glial tumors, and a prominent feature of GBMs is the occurrence of necrosis and vascular proliferation (1–3). Antiangiogenic-based therapeutic approaches seem promising in combating malignant gliomas, at least as far as experimental models are concerned (4–8). At a general level, tumor angiogenesis is regulated both by the production of angiogenic stimulators (including members of the fibroblast growth factor and the vascular endothelial growth factor families) and by angiogenic inhibitors such as angiostatin and endostatin (9). Whereas an impressive list of stimulators and inhibitors of angiogenesis has already been identified (9–11), no such effects have been reported to date for gastrin, at least to our knowledge. It was while studying the effects of gastrin on astrocytic tumor cell proliferation (12–14) and migration (13, 15–17) that we observed gastrin-mediated proangiogenic effects in experimental gliomas.[5] We describe here the *in vitro* gastrin-mediated proangiogenic effects on human umbilical vein endothelial cells (HUVECs) and the *in vivo* effects in orthotopic

Received 2/23/04; revised 8/29/04; accepted 9/16/04.
Grant support: Grants awarded by the Fonds de la Recherche Scientifique Médicale (Belgium) and the Fondation Yvonne Boël (Belgium). C. Decaestecker is a Research associate and R. Kiss is a Director of Research with the Fonds National de la Recherche Scientifique (Belgium).
The costs of publication of this article were defrayed in part by the payment of page charges. This article must therefore be hereby marked *advertisement* in accordance with 18 U.S.C. Section 1734 solely to indicate this fact.
Requests for reprints: Robert Kiss, Laboratory of Toxicology, Institute of Pharmacy (CP 205/1), Université Libre de Bruxelles, Campus Plaine, Boulevard du Triomphe, 1050 Brussels, Belgium. Phone: 32-477-62-20-83; Fax: 322-332-53-35; E-mail: rkiss@ulb.ac.be.

[5] F. Lefranc, T. Mijatovic, V. Mathieu, J. Brotchi, and R. Kiss, unpublished results.

xenografts of the human U373 glioblastoma model. Whereas HUVECs are from large vessels, neoangiogenesis in gliomas (or other tumor types) relates to microvessels. We therefore performed a cDNA microarray profiling of the interleukins (ILs) and IL receptors (IL-Rs) in HUVECs and GBM microvessels (obtained by means of a laser-assisted microscope system; ref. 18) to investigate whether HUVECs can be used as an *in vitro* model to characterize potential proangiogenic effects mediated by gastrin.

Cholecystokinin (CCK; refs. 19 and 20) and gastrin (21–23) were identified in the brain and cerebrospinal fluid about three decades ago. In fact, CCK is the most abundant peptide system in the brain, and the brain is the main production site of CCK (24). In contrast, gastrin production in the brain is limited to oxytocinergic hypothalamo-pituitary neurons and a few cerebellar and vagal neurons (24). In normal mammals, the antral G cells in the stomach and proximal duodenum are the main sites of gastrin synthesis (24). Of the various forms of gastrin found in blood or tissue, 90% are gastrin-17 (G17; ref. 24). The plasma concentrations of gastrin are more than 10 times greater than those of CCK (25). Gastrin can be produced locally as an autocrine or paracrine growth factor in various tumor types (24, 26–28), including brain tumors (29). Gastrin- and CCK-related peptides have the same biologically active COOH-terminal pentapeptide amide sequence, and gastrin can signal through several receptors and binding sites. Three receptors to which gastrin can bind have already been cloned. The CCK_A (also named CCK_1) receptor displays a high level of affinity in binding carboxyamidated and tyrosyl-sulfated CCK peptides and a low level of affinity in binding nonsulfated CCK peptides and gastrin peptides (24, 30). The CCK_B (also named CCK_2) receptor is less selective than the CCK_A receptor because it binds tyrosyl-sulfated and nonsulfated CCK peptides, gastrin, short COOH-terminal CCK, and gastrin fragments with an almost similar degree of affinity (24, 30). CCK_A and CCK_B receptors can homo- or heterodimerize (31). Gastrin can also bind to the 78-kDa gastrin-binding protein, *i.e.*, the so-called "CCK_C gastrin receptor" (32). Whereas CCK_A receptors are not expressed by glioma cells (33, 34), CCK_B receptors are expressed in low-grade glioma cells only (33). CCK_C receptors could be expressed by a large proportion of glioma cells (34). In addition to the three cloned receptors, several gastrin-binding proteins have also been described, but they have not yet been cloned. A variant of the CCK_B receptor, also labeled CCK-C (for "CCK cancer") but different from the 78-kDa CCK_C receptor, has been described in human pancreatic cancers (35). A selective receptor for glycine-extended gastrin has been described on the rat pancreatic carcinoma cell line AR4-2J (36). Singh *et al.* (37) describe a "novel" gastrin receptor, and Rehfeld *et al.* (38) show that specific binding sites for the COOH-terminal tetrapeptide of CCK or G17 exist on hog pancreatic islets. We have also identified specific binding sites for the COOH-terminal heptapeptide of gastrin on U373 human glioblastoma cells (16), which do not express CCK_A or CCK_B receptors (14, 16, 17, 34) but do express CCK_C receptor (34). We used this U373 model to investigate whether CCK_A and CCK_B receptor antagonists are able to significantly increase the survival periods of U373 orthotopic xenograft-bearing nude mice by specifically reducing neoangiogenesis in these experimental gliomas. We performed polymerase chain reaction (PCR) analyses to investigate whether CCK_A, CCK_B, and CCK_C receptor mRNAs are present in HUVECs and GBM microvessels.

IL-8 is a potent proangiogenic factor (39–41) and is stored in the Weibel-Palade body of endothelial cells, from which it can be rapidly released on stimulation by histamine or thrombin (42). Gastrin not only induces the expression of IL-8 mRNAs but also stimulates its release in human AGS gastric epithelial cancer cells (43, 44). We analyzed the influence of gastrin on IL-8 release in HUVECs. In addition, gastrin induces IL-8 expression in gastric cancer epithelial cells through the activation of nuclear factor (NF)-κB (43). We thus analyzed (*a*) whether gastrin can activate NF-κB in HUVECs (using a colorimetric-based assay for measuring NF-κB DNA binding capacity; ref. 45) and (*b*) whether specific NF-κB inhibitors can prevent gastrin-mediated tubulogenesis in HUVECs. Pagliocca *et al.* (46) show that gastrin induces branching morphogenesis in human gastric cancer AGS cells by activation of protein kinase C (PKC) and phosphatidylinositol 3′-kinase (PI3K). We investigated whether PI3K and PKC inhibitors can prevent gastrin-induced tubulogenesis in HUVECs. We then made use of computer-assisted videomicroscopy of HUVECs cultured in Dunn chambers (47) to analyze whether gastrin and IL-8 have any chemotactic influence on HUVECs.

The level of expression of E-selectin is also under the control of NF-κB (48, 49), and soluble P-selectin can induce endothelial cell migration (50). Both E- and P-selectins are induced in endothelial cells by proangiogenic cytokines such as tumor necrosis factor (TNF)-α or IL-1β (49). We thus analyzed the patterns of expression of E- and P-selectins in HUVECs both with and without stimulation by gastrin, IL-8, and IL-1β. We also used antisense oligonucleotides directed against E- and P-selectins to analyze whether E- and P-selectins are directly involved in HUVEC tubulogenesis processes.

MATERIALS AND METHODS

Experimental Cancer Cell Lines and HUVEC Primocultures

The human U373 glioma, Jurkat (clone E6-1) leukemia, and Capan-2 pancreas cancer cell lines were obtained from the American Type Culture Collection (Manassas, VA). They were maintained *in vitro* as monolayers, as detailed elsewhere (12, 14, 51). We checked the malignant astrocytic origin of the U373 model by means of a large set of markers, including the levels of expression of intermediate filaments such as nestin, vimentin, and glial fibrillary acidic protein (52) and comparative genomic hybridization analyses of 1p19q genetic alterations (51).

Human HUVECs were established to grow as *in vitro* monolayers by means of a method (53) adapted from the procedure described by Gimbrone *et al.* (54). Three distinct batches of HUVEC primocultures (Huvec 1, Huvec 2, and Huvec 3) have been used in the present work.

Compounds

Gastrin (pGlu-Gly-Pro-Trp-Leu-Glu-Glu-Glu-Glu-Glu-Ala-Tyr-Gly-Trp-Met-Asp-Phe-NH_2) and CCK [H-Asp-Tyr(SO3H)-Met-Gly-Trp-Met-Asp-Phe-NH_2] were purchased from Sigma (Bornem, Belgium). The L365,260 (3*R*-3-[*N*′-(3-methylphenyl)-

ureido]-1,3-dihydro-1-methyl-5-phenyl-2*H*-1,4-benzodiazepine-2-one) and L364,718 (3S(-)-*N*-(2,3-dihydro-1-methyl-2-oxo-5-phenyl-1*H*-1,4-benzodiazepine-3-yl-1*H*-indole-2-carboxamide) compounds were provided by ML Laboratories PLC (London, United Kingdom). Human IL-8 and IL-1β were obtained from R&D Systems (Oxon, United Kingdom). Ro320,432 (bisindolmaleimide XI; 2-(8-[(dimethylamino)methyl]-6,7,8,9-tetrahydropyrido[1,2-a]indol-3-yl)-3-(1-methylindol-3-yl)maleimide) and LY-294,002 ($C_{19}H_{17}NO_3$·HCl) were obtained from Sigma-Aldrich (Bornem, Belgium). caffeic acid phenethyl ester (CAPE), BAY-11-7085 [(*E*)-3-[(4-*t*-butylphenylsulfonyl]-2-propenenitrile] and Parthenolide ($C_{15}H_{20}O_3$) were obtained from Biomol Research Laboratories Inc. (Plymouth Meeting, PA).

In vivo Stereotactic Procedures and Treatments

Nude Rats with Surgery. The brains of 8-week–old female nude rats (150 g; Hsd:RH-nu; Harland, Horst, the Netherlands) were stereotactically grafted with 10^6 human U373 cells. The U373 glioma-bearing rats were split into three groups: one group was left untreated (control), whereas the other two groups underwent surgery to remove the bulk of their tumors (the number of grafted animals in each group is indicated in the Fig. 1 legend). The location of each tumor was established by means of nuclear magnetic resonance imaging. During the surgery carried out on the U373 glioma-bearing rats, a micropump (Alzet micro-osmotic pump; model 1002; Alza Corp., Palo Alto, CA) was installed subcutaneously on each rat's back immediately after the removal of the U373 tumor bulk. The end of the catheter was implanted directly into the brain cavity resulting from the tumor resection and maintained on the skull with cement. Illustrations of the full procedure are given elsewhere (14).

Previous experiments carried out in our laboratory revealed that when a brain tumor-bearing rat loses 10% of its weight as compared with the weight measured 3 days previously, it will die during the following 2 or 3 days (14). Each rat was therefore euthanized (by means of CO_2 inhalation) as soon as it had lost 10% of its weight as compared with the figures obtained 3 days earlier. Its brain was then removed, fixed in buffered formalin for 2 weeks, embedded in paraffin, and cut into 5-μm–thick sections, and the histologic slides were stained with hematoxylin and eosin (H&E) for vessel counts (see Fig. 1*B* and *C*). Three H&E-stained slides were analyzed for each brain, and the number of vessels like the one illustrated in Fig. 1*C* were recorded at ×400 magnification using a 10 × 10 grid fitted into the microscope eyepiece. Five fields were analyzed per slide, totaling 15 fields per U373 tumor.

Nude Mice without Surgery for Short-Term Angiogenesis-Related Analyses. The brains of thirty-five 8-week–old female nu/nu mice (21–23 g; Iffa Credo, Charles Rivers, Arbresle, France) were stereotactically implanted with 10^6 U373 cells, as detailed elsewhere (51). The 35 mice were split into seven groups of equal size 10 days after tumor graft. The first group (control) received three intracranial (through the hole of tumor cell stereotactic implantation) administrations of 20 μL saline per week (on Mondays, Wednesdays, and Fridays), for 4 consecutive weeks. The second group received twelve 20-μL intracranial administrations containing 10 mg/kg gastrin instead of saline, and the third and fourth groups received 12 administrations of 10 mg/kg L365,260 (a CCK_B receptor antagonist) and L364,718 (a CCK_A receptor antagonist), respectively. The fifth and sixth groups were the recipients of 12 concomitant administrations of G17 + L365,260 and G17 + L364,718, respectively, whereas the final group underwent twelve 20-μL intracranial administrations containing 10 mg/kg CCK-8. The administrations started at the 14th day after tumor graft, and all of the animals were euthanized on the 43rd day after tumor graft, *i.e.*, 24 hours after the final intracranial administration. The brains were processed for histology to determine the levels of angiogenesis as detailed above for the nude rats.

Unlike Schmidt *et al.* (7), we did not use Alzet osmotic minipumps because gastrin was not stable over the 28 days required for the experiments (data not shown).

Nude Mice without Surgery for Long-Term Survival– and Angiogenesis–Related Analyses. The brains of thirty 8-week–old female nu/nu mice (21–23 g; Iffa Credo, Charles Rivers) were stereotactically implanted with 10^6 U373 cells, and the mice were then split into three groups of equal size 3 days after tumor graft. The first group (control) received daily intraperitoneal administrations of 0.2 mL of saline, whereas the second and third groups received daily administrations (10 mg/kg) of either L364,718 or L365,260. The administrations started the 5th day after tumor graft. Each animal was euthanized when it had lost 10% of its weight, and, as detailed above for the nude rats, the brains were processed to determine the levels of angiogenesis.

All of the *in vivo* experiments described were performed with the authorization of the Animal Ethics Committee of the Faculty of Medicine of the Université Libre de Bruxelles (Agreement No. 55/LA 1230342).

Determination of the mRNA Expression of Gastrin/CCK Receptors, ILs, and IL-Rs in HUVECs and Vessels Microdissected from a Human Glioblastoma

Total RNA Extraction from HUVECs. Using the TRIzol isolation reagent (Life Technologies, Inc., Merelbeke, Belgium) according to the manufacturer's instructions, total RNA was extracted from the HUVEC lines under study. The RNA extracted was treated with DNase I (Life Technologies, Inc.) to eliminate any remaining genomic DNA. The quantity of RNA was measured by spectrophotometric analysis at 260 nm (Beckman Coulter DU640; Analis, Ghent, Belgium). The quality and integrity of the extracted RNA was assessed by both BioAnalyzer 2100 (Agilent, Toulouse, France) and gel electrophoresis in 1.2% agarose Tris-Acetate-EDTA (TAE) gels and visualized by ethidium bromide staining under ultraviolet (UV) light. This verification was completed by an analysis of β-actin gene expression by means of a standard reverse transcription-PCR (RT-PCR) method (see below).

Standard RT-PCR Analyses. All reverse transcription and PCR reactions were carried out in a thermal cycler (Thermocycler, Westburg, Leusden, the Netherlands). The purification of the cDNAs produced was carried out using the High Pure PCR Product Purification Kit (Roche Diagnostics, Mannheim, Germany) in accordance with the manufacturer's instructions.

As mentioned above, the integrity of the cDNA was confirmed by an analysis of β-actin gene expression on the basis of a 25-cycle PCR analysis in a total volume of 50 μL with 20 ng of loaded cDNA. All of the PCR analyses were performed on

Table 1 Description of the sense and antisense primers used in the present study

Targeted gene (human)	Sense primers	Antisense primers
β-*Actin*	5′-AAATCGTGCGTGACATTAAGG-3′	5′-CTAAGTCATAGTCCGCCTAG-3′
CCK_A receptor	5′-TGCAAACCCTTACAGTCCC-3′	5′-CCACCATCATCACACTTCC-3′
CCK_B receptor	5′-TAGCTTACCTGACACAAGAG-3′	5′-CTGTTGGTCAGAGGTATGA-3′
GBP78/CCK_C receptor	5′-AAGTCTCATCAGACGAAGAC-3′	5′-CTGTTAGCATGGTCAGCTAG-3′
IL-6	5′-GCAAACAAATTCGGTACATCC-3′	5′-GGATCAGGACTTTTGTACTCA-3′
IL-8	5′-GATCCACAAGTCCTTGTTC-3′	5′-CGTAATTCAACACAGCACTAC-3′
TNF-α	5′-GTAGCAAACCCTCAAGCT-3′	5′-GCAATGATCCCAAAGTAGAC-3′
Oncostatin M	5′-AGCATGGCGGCTATAGG-3′	5′-TCTAAGTCGGCCAGTCT-3′
gp130-oncostatin M receptor chain	5′-CTGAATCTACAGGTGAACTTC-3′	5′-TTCAAGCTGTCCGAATGTA-3′
CXCR1	5′-GACACTCAACAAGTATGTTGTG-3′	5′-GGAATTGTTTGGATGGTAAGC-3′
CXCR2	5′-GTAATTACAGTTACAGCTCTACCC-3′	5′-GCTAACATTGGATGAGTAGACG-3′

the basis of the same quantity of purified cDNA (total amount, 20 ng). The products amplified by means of the standard PCR reaction [40 cycles, except for CCK_B (50 cycles)] were resolved by gel electrophoresis in 1.2% agarose TAE gels in parallel with a 1-kb plus DNA ladder (Invitrogen, Carlsbad, CA) and visualized by ethidium bromide staining under UV light. The primers used for all of the PCR analyses (including those carried out on the microdissected vessels described below) are listed in Table 1. They were provided by Invitrogen and selected using the HYBSIMULATOR software (Advanced Gene Computing Technology, Irvine, CA). The sequencing of the PCR products was performed by GenoScreen (Lille, France) using the BigDye Terminator v3.1 Cycle Sequencing Kit (Applied Biosystems, Foster City, CA).

Microdissection of Human Glioblastoma Vessels and RNA Extraction. We used a procedure that we have detailed elsewhere (18). Briefly, a human glioblastoma was obtained immediately after surgery from the Department of Neurosurgery of the Erasmus University Hospital and directly submerged in RNAlater (Westburg). The sample was removed from the RNAlater after 24 hours at 4°C and stored frozen at −80°C until microdissection, which involved the use of a laser microscope system (P.A.L.M., Microbeam; Microlaser Technologies, AG Germany). Seven-micrometer sections were taken from the sample, and those areas containing vessels were identified on H&E-stained slides. A frozen section was then placed on a prepared slide with a membrane and colored with H&E. A total of 200 vessels (corresponding to 200 different areas of the GBM) were then excised and catapulted into the cap of a microtube, and then the cap was replaced on the tube.

The total RNA isolation from the samples obtained by microdissection was carried out by means of the RNA Isolation Kit (Biozym; Gentra Systems, Minneapolis, MN) according to the manufacturer's instructions.

RT-PCR Analysis for Microdissected Vessels. The RNA extracted was transcribed into cDNA using a SensiScript Reverse Transcriptase kit (Qiagen, Westburg; Leusden, the Netherlands) according to the manufacturer's recommendation. This procedure is specifically recommended for first-strand cDNA synthesis using less than 50 ng of RNA. The reaction was performed in a total volume of 20 μL containing 2 μL of supplied 10× concentrated buffer, 1 μL of oligo$(dT)_{12–18}$ primers (10 μmol/L), 2 μL of a supplied mix of deoxynucleotide triphosphates (5 mmol/L each), 1 μL of supplied enzyme, 1 μL of RNase inhibitor (10 units/μL), 9 μL of supplied RNase-free water, and 4 μL of extracted RNA. The mix was incubated for 60 minutes at 37°C, and the enzyme was inactivated by heating the reaction mixture at 93°C for 5 minutes before rapid cooling on ice. The products of 10 reverse transcription reactions were pooled and stored at −80°C.

The integrity of the cDNA was confirmed by an analysis of β-actin gene expression on the basis of a 45-cycle PCR method in a total volume of 25 μL containing 5 μL (one fourth of one reverse transcription reaction) of loaded cDNA. The absence of contamination by genomic DNA was verified by means of the PCR analysis of β-actin gene expression in a nontranscribed RNA sample. The evaluation of the expression of the different mRNAs under study was performed by means of a 50-cycle PCR method in a total volume of 25 μL containing 5 μL (one fourth of one reverse transcription reaction) of loaded cDNA. The remaining steps ($MgCl_2$ concentration, annealing temperature, electrophoresis, and visualization) were similar to those performed in standard RT-PCR analyses (see above).

Complementary DNA Microarray Assays. We used two types of microarrays provided by Superarray (Bethesda, MD) and referenced as the GEArray Original Series Human Common Cytokine Gene Array and the GEArray Original Series Human Interleukin Receptor Gene Array, respectively. Whereas the former was designed to assess the levels of expression of 23 common cytokines, the latter was specifically concerned with the level of expression of 23 interleukin receptors (spotted in duplicate). A complete description of these arrays can be found in files xpd_hGEA9912090.pdf and xpd_hGEA9913020.pdf on-line.[6] The array kits were used in accordance with the procedures recommended by the manufacturer on-line[7] to assess the levels of gene expression in equal amounts of total RNA extracted from untreated HUVECs. The hybridization results were visualized using a Fuji-BAS5000 scanner and AIDA image analyzer software (Raytest Benelux, Tilburg, the Netherlands).

Enzyme-Linked Immunosorbent Assay Tests

HUVEC culture supernatants were collected after different treatments and periods of time. Separate aliquots of these su-

[6] http://www.superarray.com/gene_array_product/.
[7] http://www.superarray.com/support_manual.php).

pernatants were stored at −20°C. Two different human enzyme-linked immunosorbent assay (ELISA) kits were used in our study (in accordance with the procedures recommended by the manufacturers), namely, Human IL-1β Quantikine and Human IL-8 Quantikine Parameter ELISA Kits (R&D Systems). Each sample was assessed in triplicate.

NF-κB DNA Binding Assay

NF-κB DNA binding activity was assessed with *trans*-active motif (*trans*-AM) NF-κB family transcription factor assay kits (Active Motif Europe, Rixensart, Belgium) according to the manufacturer's instructions. This ELISA-like test measures the level of the active form of NF-κB contained in cell extracts specifically able to bind to an oligonucleotide containing the NF-κB consensus site (5′-GGGACTTTCC-3′) attached to a 96-well plate (45). Whole cell lysates were prepared after G17 treatment, and 20-μg extracts were added to the 96-well plates. The binding of NF-κB to the DNA was visualized by anti-p50, anti-p52, anti–p65/Rel-A, anti–Rel-B, and anti–c-Rel antibodies that specifically recognize activated NF-κB (45). Antibody binding was determined as absorbance values at 450 nm (45).

HUVEC Capillary-Like Structure Formation

Twenty-four–well culture plates (Nunc, Nalge Europe; Neerijse, Belgium) were coated with 250 μL of Matrigel (BD Biosciences), a basement membrane matrix liquid at 4°C, which was then allowed to solidify at 37°C for 30 minutes. The HUVECs growing as primocultures in 25-mm^2 flasks (Nunc) were trypsinized, counted, suspended in a culture medium, and added to the Matrigel-coated wells (100,000 cells per well in 900 μL of medium). Different compounds (see Results) were added to the HUVEC suspensions just before seeding onto the Matrigel support. The HUVECs were incubated for 10 hours at 37°C, and digitized pictures were made (with a computer-assisted phase-contrast Olympus IX50 microscope; Omnilabo SA, Antwerp, Belgium) every 2 minutes (during this 10-hour period of observation) to determine the influence of these compounds on the ability of the HUVECs to form tubule-like structures. Each experimental condition was carried out in triplicate.

The E-selectin antisense and scrambled oligonucleotides took the form of 5′-fluo-GCTAAGTTAATGGAAGT-phosphorothioate-3′ (antisense) and 5′-fluo-AGTAGGGCATAAGTTTA-phosphorothioate-3′ (scrambled), whereas 5′-fluo-GCTATTGGCTTATTAAC-phosphorothioate-3′ (antisense) and 5′-fluo-CAATTATTCGGTTATCG-phosphorothioate-3′ (scrambled) constituted the P-selectin antisense and scrambled oligonucleotides. These four oligonucleotides, purchased from BioSource Europe (Nivelles, Belgium), were also selected using HYBSIMULATOR software (Advanced Gene Computing Technology).

Quantitative Determination of G17- and IL-8–Induced Chemotactic Effects on HUVECs

Chemotaxis was assessed by the direct observation and recording of cell behavior in stable concentration gradients of G17 or IL-8 established in Dunn chemotaxis chambers (Weber Scientific International Ltd., Teddington, United Kingdom). As detailed elsewhere (47), these chambers have two concentric wells separated by an annular platform and enable radially directed linear diffusion gradients to be established. The cells were cultured on a coverslip that was then inverted onto a glass slide. The cells attached to the annular platform were observed under a phase-contrast microscope and recorded automatically by an acquisition system described elsewhere (47). A software that we had previously developed enables the αMRDO parameter to be quantitatively determined; MRDO represents the maximum relative distance traveled by each cell from its point of origin during a 24-hour period of observation, whereas αMRDO is the vector joining the original point of a cell trajectory to the farthest point reached. We analyzed the distribution of the angular directions of these vectors to evidence a possible chemotactic effect of G17 as compared with IL-8 (see Statistical Analyses).

Computer-Assisted Fluorescence Microscopy for Determination of the Levels of Expression of E- and P-Selectin in HUVECs

The levels of expression and/or patterns of activation of E-selectin and P-selectin were quantitatively determined by means of computer-assisted fluorescence microscopy (as detailed elsewhere; ref. 52) carried out on HUVECs cultured on gelatin substrates and treated with either G17, IL-8, or IL-1β (as detailed in the figure legends) or left untreated (control). The anti–E-selectin and anti–P-selectin antibodies were purchased from R&D Systems. The HUVEC suspensions were seeded onto glass coverslips 48 hours before immunofluorescence staining; the cells were then fixed with 4% formaldehyde in PBS (pH 7.4) for 20 minutes. Three coverslips were available for each experimental condition. The cells were not permeabilized and were incubated for 1 hour at room temperature with the various primary and secondary antibodies.

The levels of expression and/or patterns of activation of the two selectins (relative to the fluorescence staining intensity) were determined quantitatively by means of a PROVIS Olympus Microscope (Omnilabo SA) coupled to a Megaview 2 camera (Omnilabo SA) feeding digitized information to a computer using AnalySIS software (Soft Imaging System, GMbH, Munster, Germany). One hundred cells were analyzed per cell line for each of the markers under study.

Statistical Analyses

Statistical comparisons between the control and the treated groups were made by first carrying out the Kruskal-Wallis test (a nonparametric one-way analysis of variance), and where this test revealed significant differences, we investigated whether any of the treated groups differed from control. For this purpose, we applied the Dunn multiple comparison procedure (two-sided test) adapted to the special case of comparisons of treatments and control, *i.e.*, where only $(k - 1)$ comparisons were made among the k groups tested by the Kruskal-Wallis test [instead of the possible $k(k - 1)/2$ comparisons considered in the general procedure (55, 56)].

Survival analysis was performed by using Kaplan-Meier curves and Gehan's generalized Wilcoxon test. All these statistical analyses were carried out using Statistica (Statsoft, Tulsa, OK).

To study the impact of a potentially chemoattractive agent (say G17 or IL-8) on cell displacements, we analyzed its influence on the distribution of the αMRDO vectors used to characterize the directions of the cell trajectories (see above). The standard Rayleigh test (57) was used for this purpose (using an algorithm that we developed).

RESULTS

***In vivo* Effects of G17 and CCK-8 on U373 Glioma Neoangiogenesis.** Fig. 1*A* illustrates the histopathological pattern of a human U373 glioma (*T*) implanted into the brain (*B*) of a nude rat. Fig. 1*B* shows the presence of pseudopalisading processes with necrosis (*N*), and the *arrow* points to a microvessel further magnified in Fig. 1*C*. As illustrated in Fig. 1*C*, determination of the levels of angiogenesis depends on the count of this type of microvessel. In sharp contrast, we did not take into account the types of vessels illustrated in Fig. 1*G* for the reasons explained below.

The continuous delivery by means of a micropump of G17 (Fig. 1*D*, *S+G*) into the surgical resection cavity significantly increased neoangiogenesis in both the tumor bulk (Fig. 1*D*, ■) and the peritumoral areas (Fig. 1*D*, ▩) of the U373 gliomas implanted into the brains of the nude rats, but not in normal brain tissues (Fig. 1*D*, □), as compared with saline (Fig. 1*D*, *S+S*) or with an actual control group of untreated U373 gliomas (Fig. 1*D*, *CT*).

Twelve intracranial administrations of G17 (Fig. 1*E*, *G17*) significantly increased the levels of neoangiogenesis in the U373 experimental GBMs as compared with the same type of delivery for saline (Fig. 1*E*, *Control*). Twelve intracranial administrations of either L365,260 or L364,718 did not significantly modify the levels of neoangiogenesis in the orthotopic U373 gliomas. In contrast, the daily intraperitoneal administration of L365,260, but not L364,718, for about 2 months (thus about 40 intraperitoneal administrations of L365,260) significantly decreased these angiogenesis levels (Fig. 1*I*), with a concomitant L365,260-induced increase in the survival periods of the U373 orthotopic xenograft-bearing nude mice, a feature not observed in the case of L364,718 (Fig. 1*H*). L365,260 significantly antagonized the G17-induced proangiogenic effects (Fig. 1*E*, *L365 + G17*), a feature not observed with L364,718 (Fig. 1*E*, *L364 + G17*). CCK-8 induced only weak proangiogenic effects as compared with G17 (Fig. 1*E*), a fact that encouraged us to pursue our investigations with G17 alone.

As illustrated in Fig. 1*G*, in many of the gastrin-treated tumors (about 70%), we observed large lacunae full of blood, a feature that was not observed in the control tumors (Fig. 1*F*). These lacunae could correspond to gastrin-induced sprouting of endothelial cells, but with the incomplete vessel formation that can be seen in many types of tumors (58).

Characterization of Expression of CCK_A, CCK_B, and CCK_C Receptor, IL and IL-R mRNAs, and CXCR1 and CXCR2 mRNAs in HUVECs and in Vessels Microdissected from a Human Glioblastoma. As illustrated in Fig. 2*A−C*, we observed strong mRNA expression for the CCK_A, CCK_B, and CCK_C receptors in three independent HUVEC primocultures; the mRNA expression for these receptors was also evidenced in the microvessels microdissected from a human glioblastoma (Fig. 2*E−G*). All of the PCR products were checked by means of sequencing (data not shown).

The patterns of expression of the ILs and their receptors (IL-Rs) were characterized in HUVECs by means of two different cDNA microarrays. Fig. 2*I* shows that the IL-8 mRNAs were markedly present in HUVECs (as they were in the GBM microdissected microvessels; Fig. 2*P*), whereas Fig. 2*J* indicates that the IL-8 receptor [*i.e.*, CXCR1 (IL-8 receptor α) and CXCR2 (IL-8 receptor β)] mRNAs were not present in the HUVECs. The absence (or only very weak presence) of CXCR1 and CXCR2 mRNAs was further confirmed by means of standard PCR analyses (Fig. 2*K* and *L*).

TNF-α (Fig. 2*N*) and IL-8 (Fig. 2*P*) mRNAs were detected in the vessels microdissected from a human glioblastoma, but no IL-6 (Fig. 2*O*), gp130-oncostatin-M receptor chain (Fig. 2*Q*), or oncostatin M (Fig. 2*R*) mRNA was detected.

Characterization of the Influence of G17 and CCK_B (and CCK_A) Receptor Antagonist on the Ability of HUVECs to Form Capillary-Like Structures *In vitro*. HUVECs form capillary-like structures when they are plated on Matrigel, as illustrated in Fig. 3*A* ($t = 0$ h) and *B* ($t = 2$ h), but they remain individual when plated in a Dunn chamber (without Matrigel, but on gelatin), as illustrated in Fig. 3*C* ($t = 0$ h) and *D* ($t = 8$ h).

Fig. 3*B* illustrates our method of analysis of angiogenesis [*i.e.,* by counting the number of branches (*b*) present on a 1,000-μm^2 surface at ×20 magnification]. Fig. 3*B* shows that 11 branches (*b1–b11*) were present in the field that we analyzed. For each experimental condition, we analyzed six fields like the one illustrated in Fig. 3*B*. Each experiment was performed in triplicate.

Fig. 3*E* shows that 10 nmol/L G17 (■) significantly increased the rate at which the HUVECs formed tubulogenesis as compared with control (▩). Whereas G17 at 0.01 nmol/L caused no statistically significant effects on HUVEC capillary-like formation as compared with control, the data obtained with 0.1 and 1 nmol/L were similar to but weaker than those illustrated in Fig. 3*B* (at 10 nmol/L; data not shown). The G17-mediated effects on HUVEC tubulogenesis at 100 nmol/L were not higher ($P < 0.05$) than those observed at 10 nmol/L (see Fig. 4*A*). At 10 nmol/L, L365,260 (a CCK_B receptor antagonist) did not have any effect by itself, nor did it antagonize the G17-mediated effects (data not shown). In contrast, 100 nmol/L L365,260 completely antagonized the G17-mediated proangiogenic effects, a feature not observed with 100 nmol/L L364,718 (Fig. 3*F*).

Characterization of PI3K (LY294,002) and PKC (Ro320,432) Inhibitors on G17-Mediated Effects on HUVEC Tubulogenesis. G17 significantly increased the tubulogenesis levels in the HUVECs cultured for 7 hours on Matrigel as compared with control (Fig. 4*A*); the effects observed at 100 nmol/L were similar ($P > 0.05$) to those observed at 10 nmol/L (Fig. 4*A*). Whereas 10 μmol/L LY294,002 induced no statistically significant effects on the HUVEC tubulogenesis, 50 μmol/L LY294,002 slightly, but nevertheless significantly ($P < 0.05$), decreased it (Fig. 4*A*). Whereas the addition of 10 μmol/L LY294,002 one hour before 10 nmol/L G17 brought about a slight decrease in HUVEC tubulogenesis, the addition of 50 μmol/L LY294,002 one hour before 10 nmol/L G17 provoked a significant decrease (Fig. 4*A*). Increasing the concentration of G17 from 10 to 100 nmol/L blocked the L294,002-induced

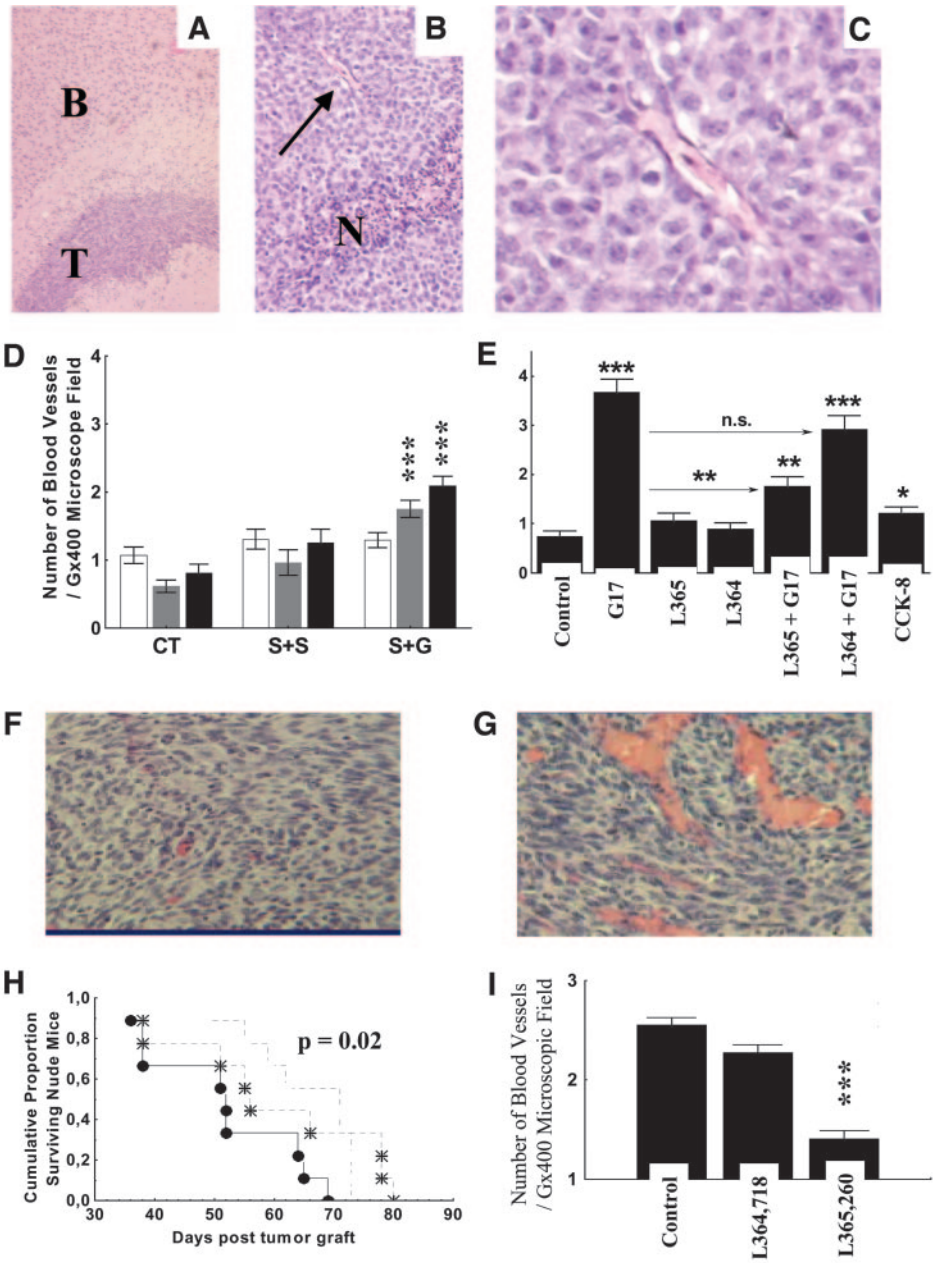

Fig. 1 Influence of gastrin and CCK receptor antagonists on experimental glioma models. *A* (×100), *B* (×200), and *C* (×400) illustrate the morphologic patterns of the U373 glioma model orthotopically xenografted into the brain of a nude rat and show the type of vessel taken into account to determine the levels of angiogenesis (*C*). *D* reports data on the angiogenesis levels in the U373 glioma models implanted into nude rats. The CT group ($n = 7$) contains the rats that did not undergo surgery and did not receive any gastrin or saline delivery. The S+S and S+G groups contain the rats that underwent surgery with micropump delivery of either saline (*S+S*; $n = 7$) or 10^{-8} mol/L gastrin (*S+G*; $n = 6$) for 7 days. □, normal brains, ▨, peritumoral areas; ■, tumor areas. The data are presented as the means (*thick bars*) ± SE (*thin bars*) of the number of blood vessels per histopathological fields analyzed at a ×400 magnification (***, $P < 0.001$ compared with control). *E* describes the effects of 12 intracranial administrations (for 4 weeks) of 10 mg/kg G17, 10 mg/kg L365,260 (*L365*), 10 mg/kg L364,718 (*L364*), the combination of G17 and L365,260 (*L365 + G17*), the combination of G17 and L364,718 (*L364 + G17*), and 10 mg/kg CCK-8 on the levels of angiogenesis in U373 gliomas orthotopically implanted into the brains of nude mice. *F* and *G* illustrate the morphologic patterns of U373 gliomas under control and G17-treated conditions (×200). *H* illustrates the survival periods of U373 glioma-bearing nude mice treated with either L364,718 (a CCK_A receptor antagonist; *stars*) or L365,260 (a CCK_B receptor antagonist; no symbol) as compared with untreated animals (control, ●). *I* represents the determination of the levels of angiogenesis (performed as described in *D* and *E*) in U373 gliomas (corresponding to the survival curves in *H*) obtained from animals treated with L364,718 or L365,260 or left untreated (*Control*). The data are presented as means (*bars*) ± SE (*thin bars*), with *** = $P < 0.001$ (as compared with control).

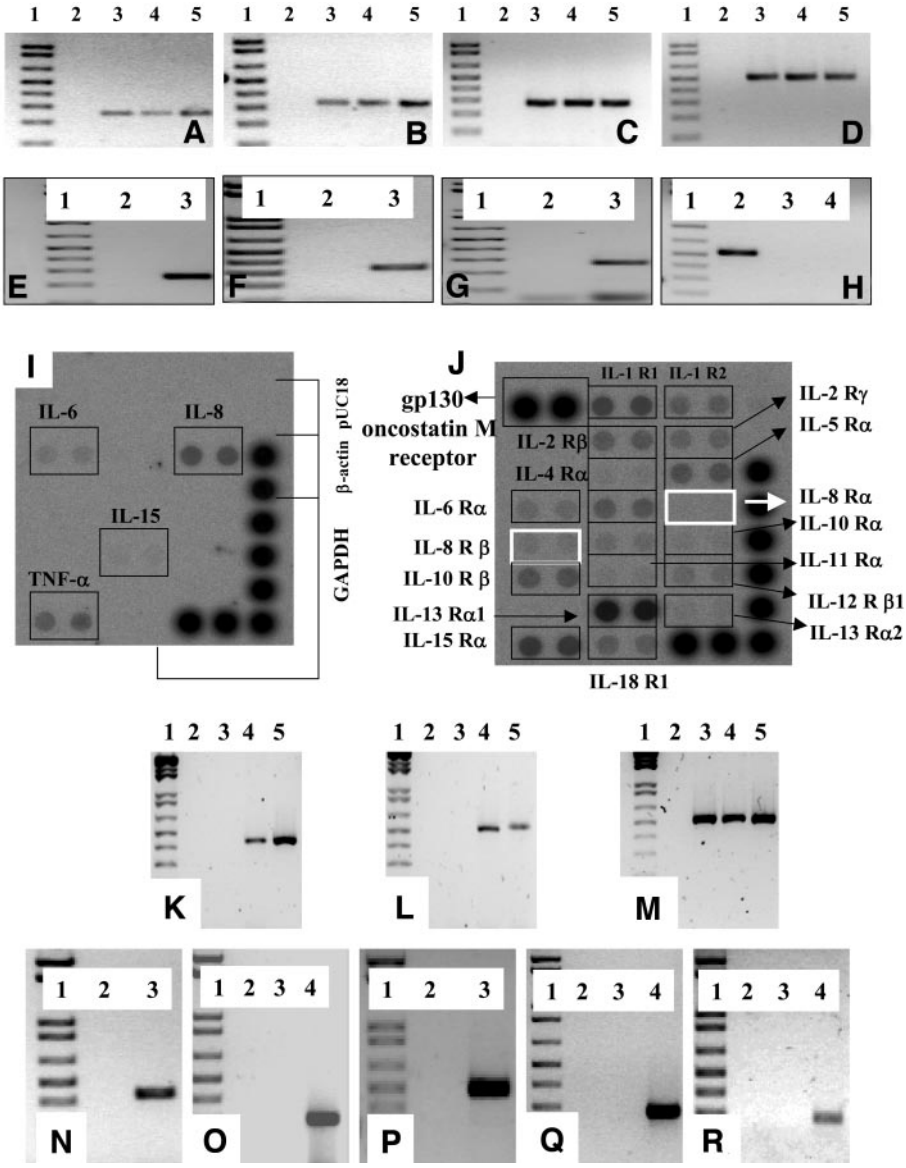

Fig. 2 Expression of CCK receptor, IL, and IL-R mRNAs in HUVECs and vessels from a human glioblastoma. The detection of mRNAs (by means of RT-PCR) for CCK_A (*A*; *Lanes 3–5*; 252 bp), CCK_B (*B*; *Lanes 3–5*; 332 bp), and CCK_C (*C*; *Lanes 3–5*; 271 bp) in three different HUVEC primocultures (Huvec 1, Huvec 2, and Huvec 3). *D* shows the detection of β-actin mRNAs (*Lanes 3–5*; 525 bp) in these three primocultures. Whereas *Lane 1* in *A*−*D* shows the DNA size ladder, *Lane 2* corresponds to the nontemplate control (H_2O). *E*−*G* (*Lane 3*) show the presence of mRNAs for CCK_A, CCK_B, and CCK_C, respectively, and *H* (*Lane 2*) shows the presence of mRNAs for β-actin (respectively) detected in vessels microdissected from a human glioblastoma. Whereas *Lane 1* in *E*−*H* gives the 1-kb plus DNA size ladder, *Lane 2* in *E*−*G* and *Lane 4* in *H* correspond to the nontemplate control. *Lane 3* in *H* corresponds to nontranscripted RNA. *I* and *J* illustrate the use of cDNA microarrays to characterize the presence or the absence of IL and IL-R mRNAs in the HUVECs (Huvec 1). *K*−*M* confirm (see *J*) the absence of CXCR1 [IL-Rα; *K*; 40 cycles; *Lane 1* = DNA ladder, *Lane 2* = control without cDNA, *Lane 3* = HUVEC cDNA, *Lane 4* = Capan-2 human pancreatic cancer (positive control), and *Lane 5* = Jurkat human leukemia (positive control); 445 bp] and CXCR2 (IL-Rβ; *L*; 40 cycles, *Lanes 1–5* as described for *K*; 518 bp) mRNAs in the HUVECs (Huvec 2) by means of a RT-PCR analysis (*M* represents β-actin analysis as a control quality; 25 cycles; *Lanes 1–5* as described for *K*). *N*−*R* illustrate the PCR analyses performed on GBM microvessels obtained by means of microdissection: TNF-α (*Lane 3* in *N*; 419 bp), IL-6 [*Lane 3* in *O*; 295 bp; with *Lane 4* corresponding to the HUVECs (Huvec 2) taken as positive control], IL-8 (*Lane 3* in *P*; 508 bp), the gp130 oncostatin M receptor chain (*Lane 3* in *Q*; 284 bp; with *Lane 4* corresponding to Huvec 2), and oncostatin M (*Lane 3* in *R*; 272 bp; with *Lane 4* corresponding to Huvec 2). Whereas *Lane 1* in *N*−*R* shows the 1-kb plus DNA size ladder, *Lane 2* corresponds to the nontemplate control (H_2O).

inhibitory effects on HUVEC tubulogenesis (Fig. 4*A*). These data suggest that PI3K plays a major role in the G17-mediated effects on HUVEC tubulogenesis features. Fig. 4*B* illustrates the morphologic appearance of HUVEC tubulogenesis 7 hours after the addition of 10 nmol/L G17 to the culture media, whereas Fig. 4*C* illustrates the morphologic appearance of the HUVECs coated on Matrigel, where 50 μmol/L LY294,002 has been added to the culture medium 1 hour before 10 nmol/L G17. Fig.

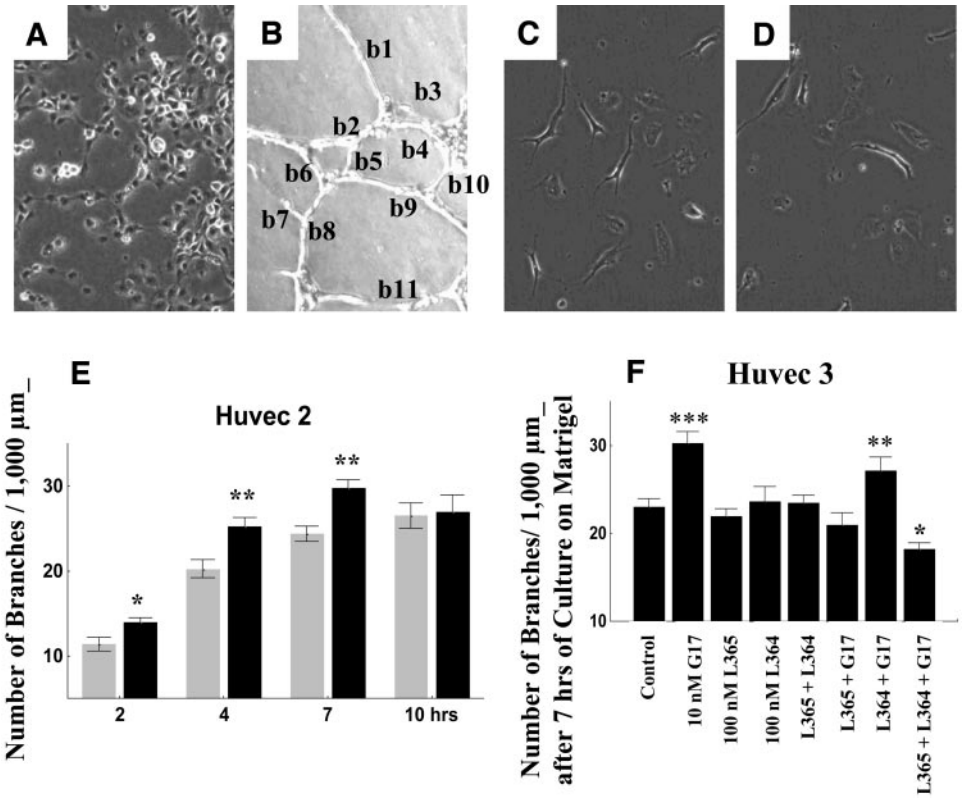

Fig. 3 Influence of G17 and CCK receptor antagonists on the ability of HUVECs to form capillary-like structures. *A* and *B*, illustration of the pattern of capillary-like structures formed by control HUVECs (Huvec 2) 0 (Fig. 3A) and 2 hours (Fig. 3B) after the plating of these endothelial cells on Matrigel. *C* and *D*. HUVECs remain individual when cultured on gelatin ($C = 0$ hours of culture on gelatin; $D = 8$ hours of culture on gelatin). *E*, determination of the effects of 10 nmol/L G17 (■) on the levels of capillary-like structure formation with respect to control (▨) in Huvec 2 primocultures. The cells were plated at $t = 0$ hours, and the number of structures per 1,000 μm^2 (see *B*) were recorded after 2, 4, 7, and 10 hours of culture of the HUVECs on Matrigel. *F*, characterization of 10 nmol/L G17; 100 nmol/L L365,260; 100 nmol/L L364,718; 100 nmol/L L365,260 and 100 nmol/L L364,718 (*L365 + L364*); 100 nmol/L L365,260 followed 30 minutes later by 10 nmol/L G17 (*L365 + G17*); 100 nmol/L L364,718 followed 30 minutes later by 10 nmol/L G17 (*L364 + G17*); and 100 nmol/L L365,260 and 100 nmol/L L364,718 followed 30 minutes later by 10 nmol/L G17 (*L365 + L364 + G17*) on the levels of capillary-like structure formation with respect to control in Huvec 3 primocultures. The quantitative data are presented as means (*bars*) ± SE (*thin bars*), with * = $P < 0.05$, ** = $P < 0.01$, and *** = $P < 0.001$ (as compared with control).

4*C* clearly shows that the HUVECs treated with 50 μmol/L LY294,002 one hour before 10 nmol/L G17 were alive, but they were no longer capable of undergoing tubulogenesis. Fig. 4*D* shows that Ro320,432 significantly decreased HUVEC tubulogenesis, probably through inhibition of the culture medium growth factor-mediated activation of this tubulogenesis. The fact that the concomitant addition of Ro320,432 and G17 only slightly decreased the G17-mediated effects on the HUVEC tubulogenesis suggests that the PKC signaling pathways were only marginally involved in the G17-mediated effects on HUVEC tubulogenesis. On the contrary, G17 was potent enough to antagonize the Ro320,432-induced inhibitory effects on HUVEC tubulogenesis (Fig. 4*D*).

Characterization of G17-Induced Effects on IL-8 Secretion by HUVECs and on NF-κB–Mediated IL-8 Secretion and Potential NF-κB–Mediated Effects on HUVEC Tubulogenesis. G17 did not significantly ($P > 0.05$) increase IL-8 release (secretion) from HUVECs 2 hours after the addition of G17 to the HUVEC culture (Fig. 5*A*, ▨). In contrast, G17 markedly ($P < 0.001$) stimulated IL-8 release from HUVECs 12 hours after the addition of G17 to the culture media (Fig. 5*A*, ■). Thus, the G17-mediated increase in the HUVEC tubulogenesis process (see Fig. 3) cannot be related to a G17-induced release of IL-8 from the HUVECs because G17 had already significantly increased HUVEC tubulogenesis 2 hours after the addition of G17 to the culture media (Fig. 3*D*), whereas G17 had not significantly increased IL-8 release from the HUVECs by then (Fig. 5*A*). G17 (10 nmol/L) did not significantly activate NF-κB DNA binding activity during the first 2 hours after addition of G17 to the HUVEC culture media (Fig. 5*B*).

Fig. 5*C* schematically illustrates where on the NF-κB pathway (see explanations in Discussion) the three inhibitors Parthenolide, BAY-11-7085, and CAPE, specifically have an inhibitory effect. Fig. 5*D* shows that G17 significantly increased HUVEC tubulogenesis 10 hours after its addition to the culture media. Whereas the G17-induced increase in HUVEC tubulogenesis was not antagonized by CAPE, it was slightly antagonized by Parthenolide and BAY-11-7085 only (Fig. 5*D*).

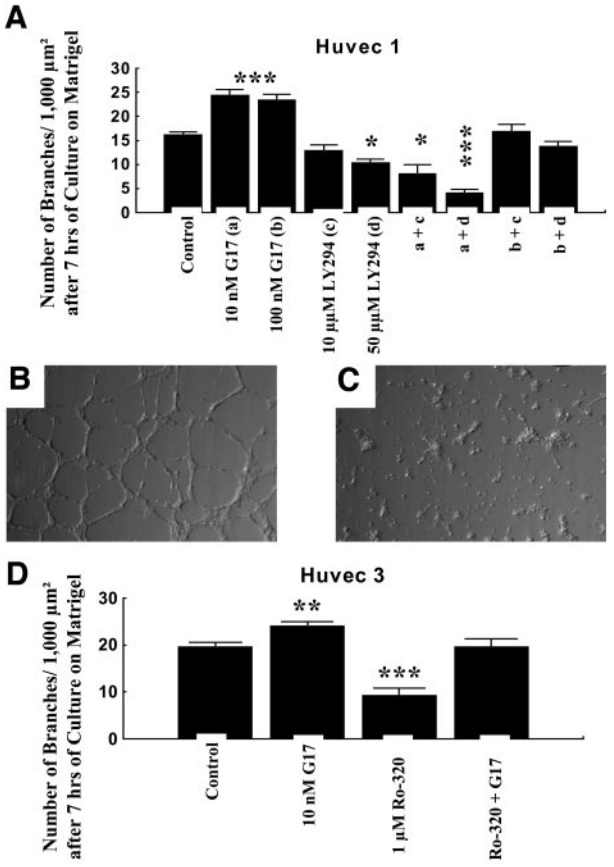

Fig. 4 Effects *in vitro* of PI3K and PKC inhibitors on G17-mediated proangiogenic influence. *A* shows the effects of 10 and 100 nmol/L G17 on the HUVEC tubulogenesis process in comparison with the effects induced by 10 and 50 μmol/L LY294,002 (a PI3K inhibitor), alone or in combination with G17. *B* and *C* illustrate the morphologic pattern (×20; phase-contrast microscopy) of HUVEC tubulogenesis in the presence of 10 nmol/L G17 for 7 hours or in the presence of 10 nmol/L G17 and 50 μmol/L LY294,002 for 7 hours. *D* illustrates the effects of 10 nmol/L G17 on the HUVEC tubulogenesis process in comparison with the effects induced by 1 μmol/L Ro320,432 (a PKC inhibitor), alone or in combination with G17. The quantitative data are presented as means (*bars*) ± SE (*thin bars*), with ** = $P < 0.01$ and *** = $P < 0.001$ (as compared with control).

Characterization of G17–, IL-1β–, and IL-8–Induced Chemotactic Effects on HUVEC Migration. The chemotactic-related experiments into G17 and IL-8 were carried out independently and in triplicate, with about 300 cell trajectories analyzed in each of the experimental conditions (after pooling). These trajectories are illustrated in Fig. 6*A*, in which each *colored line* corresponds to a path traveled by an individual HUVEC (see Fig. 3*C* and *D*) over an 8-hour observation period. In Fig. 6*B*, all of the initial cell positions are set to the origin (0, 0) of the axes, and the trajectories are reported in terms of gradient direction. The gradient direction is arbitrarily fixed in an easterly direction (the *red dot* highlighted by the *red arrow*). The *red arrows* in Fig. 6*C* and *D* thus indicate the point where either saline (control) or 10 nmol/L G17 was added. Each individual HUVEC trajectory is characterized by means of its αMRDO vector (joining the initial and most distant cell positions) in Fig. 6*C* and *D* (*blue arrows*). These figures also compare the resulting direction of all of the αMRDO vectors (*green arrows*) with the gradient direction (*red arrows*). Fig. 6*C* and *D* clearly show that G17 had a chemotactic effect on the HUVECs. Rayleigh statistical test analyses applied to the computer-assisted microscope quantification of these directional motility features revealed that G17 significantly chemoattracted the HUVECs at 0.1 ($P < 0.001$), 1 ($P < 0.001$), and 10 nmol/L ($P < 0.01$), but not at 100 nmol/L ($P > 0.05$). We did not test whether concentrations of <0.1 nmol/L G17 still chemoattracted the HUVECs. Neither IL-8 nor IL-1β significantly chemoattracted the HUVECs over concentrations ranging from 0.01 to 10 nmol/L (data not shown).

Characterization of G17-Induced Modifications to the Actin Cytoskeleton Organization in HUVECs. Fig. 6*E* illustrates the morphologic aspect of the actin cytoskeleton in the untreated HUVECs (the *0* experimental condition in Fig. 6*H*). The presence of fibrillary actin was revealed by *green fluorescence*, and that of globular actin was revealed by *red fluorescence*. Fig. 6*F* and *G* illustrate the appearance of the actin cytoskeleton of HUVECs cultured in the presence of 10 nmol/L G17 for 3 and 6 hours, respectively, a feature indicating a marked G17-induced depolymerization of the fibrillary actin. The use of computer-assisted fluorescence microscopy made it possible to compute the ratio of fibrillary/globular actin, as shown in Fig. 6*H*. This demonstrates that the G17-induced modifications to the actin cytoskeleton organization occurred mainly during the first 6 hours after the addition of G17 to the HUVEC culture media.

Characterization of G17–, IL-8–, and IL-1β–Induced Effects on E- and P-Selectin Expression in HUVECs, with Emphasis on the Potential Roles of E- and P-Selectins in HUVEC Migration Features. The influence of G17, IL-1β, and IL-8 on the levels of expression of E- and P-selectin in the HUVECs was determined quantitatively by means of computer-assisted fluorescence microscopy. Fig. 7*A* and *B* illustrate the patterns of E-selectin expression in an untreated HUVEC and in a HUVEC treated with 10 nmol/L G17 for 6 hours. In accordance with these patterns, quantitative immunofluorescence revealed that at 10 nmol/L, G17 (Fig. 7*C*, *red bars*) dramatically but transiently decreased the levels of E-selectin in the HUVECs. Because we did not permeabilize HUVEC membrane during the E-selectin cytochemical staining process, this G17-induced transient disappearance of E-selectin on the surface of the HUVECs could correspond to a G17-induced internalization process of E-selectin rather than to an actual G17-induced decrease in E-selectin expression. G17 (Fig. 7*C*, *blue bars*) began by slightly decreasing the levels of expression (or by slightly activating the internalization process) of P-selectin in the HUVECs and then dramatically stimulated P-selectin expression and/or the activation processes. As revealed by an ELISA (data not shown), the G17-induced decrease in E- and P-selectin levels of expression in the HUVECs (during the first 6 hours after their addition to the culture medium; see Fig. 7*C*) did not correspond to a G17-induced increase in E- and P-selectin secretion by the HUVECs into their culture media. These G17-induced transient decreases in E- and P-selectin might therefore correspond to a G17-induced internalization of

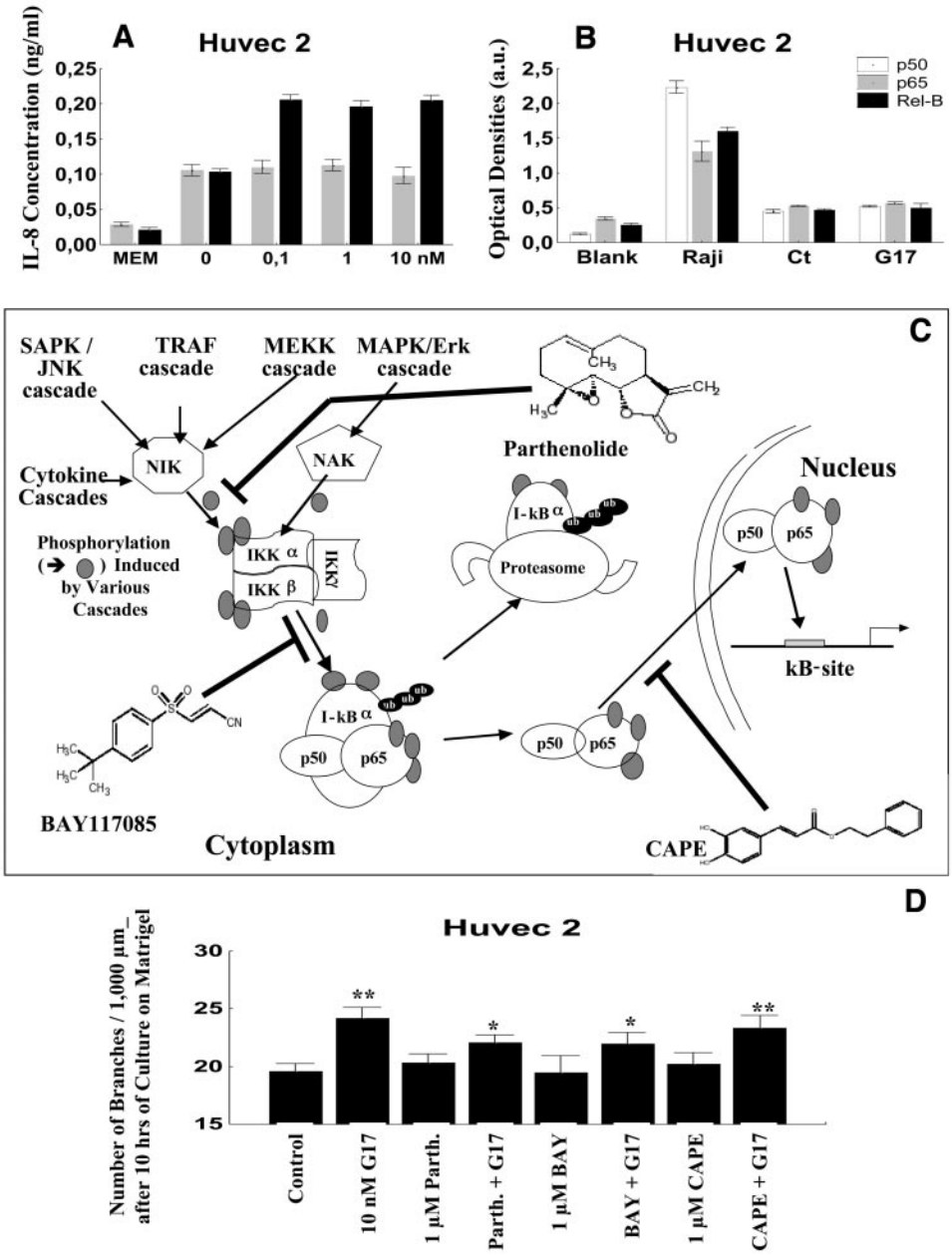

Fig. 5 Effects of G17 on IL-8 release by HUVECs and on NF-κB activation and characterization of the effects of NF-κB inhibitors on G17-mediated *in vitro* proangiogenic effects. *A*, influence of 0 (control), 0.1, 1, and 10 nmol/L G17 for 2 (▨) or 12 hours (■) on IL-8 release (secretion) by HUVECs. *B*, characterization of the influence of 10 nmol/L G17 for 2 hours as compared with control (*Ct*) on NF-κB DNA binding activity (p50, p65/Rel-A, and Rel-B subunits). The Raji lymphoblast-like cells were used as a positive control of the methodology, in comparison with basal values (*Blank*) obtained by means of the *trans*-AM NF-κB family transcription factor assay kit. *C*, schematic illustration of the activation of the NF-κB pathway with the precise antagonistic effects of Parthenolide, BAY-11-7085, and CAPE. *D* illustrates the effects of 10 nmol/L G17 on HUVEC tubulogenesis compared with the effects induced by 1 µmol/L Parthenolide, 1 µmol/L BAY-11-7085, and 1 µmol/L CAPE alone (see *C*) or in combination with G17. The quantitative data in *A*, *B*, and *D* are presented as means (*bars*) ± SE (*thin bars*), with * = $P < 0.05$ and ** = $P < 0.01$ (as compared with control).

E- and P-selectin, as already suggested above in connection with the fact that no permeabilization procedure was used during the cytochemical staining process.

The addition of a CCK_B receptor antagonist (L365,260) or a CCK_A receptor antagonist (L364,718) for 6 hours at 10 nmol/L did not prevent the G17-induced decrease in E-selectin membrane expression in the HUVECs (data not shown). In contrast, the addition of both L364,718 and L365,260 at 10 nmol/L for 6 hours completely blocked any G17 effects (data not shown). L364,718 and L365,260, either singly or combined, did not prevent the G17-induced decrease in P-selectin expression (data not shown), a fact that could suggest the implication of another gastrin receptor or gastrin-binding protein in these G17-mediated modifications to the P-selectin membrane expression in the HUVECs.

IL-1β (Fig. 7*D*, ▨) and IL-8 (Fig. 7*D*, ■) significantly increased the levels of expression of E-selectin in the HUVECs, but did not significantly increase the levels of expression P-selectin in the HUVECs (data not shown).

We used an antisense oligonucleotide approach (Fig. 7*E* and *F*) to decrease the levels of E- and P-selectin (Fig. 7*G*) membrane expression in the HUVECs to investigate the influence of this decrease on the ability of the HUVECs to form capillary-like structures. We made use of green fluorescent scrambled or antisense oligonucleotides and showed the presence of E- or P-selectin under red fluorescence (Fig. 7*E*). We

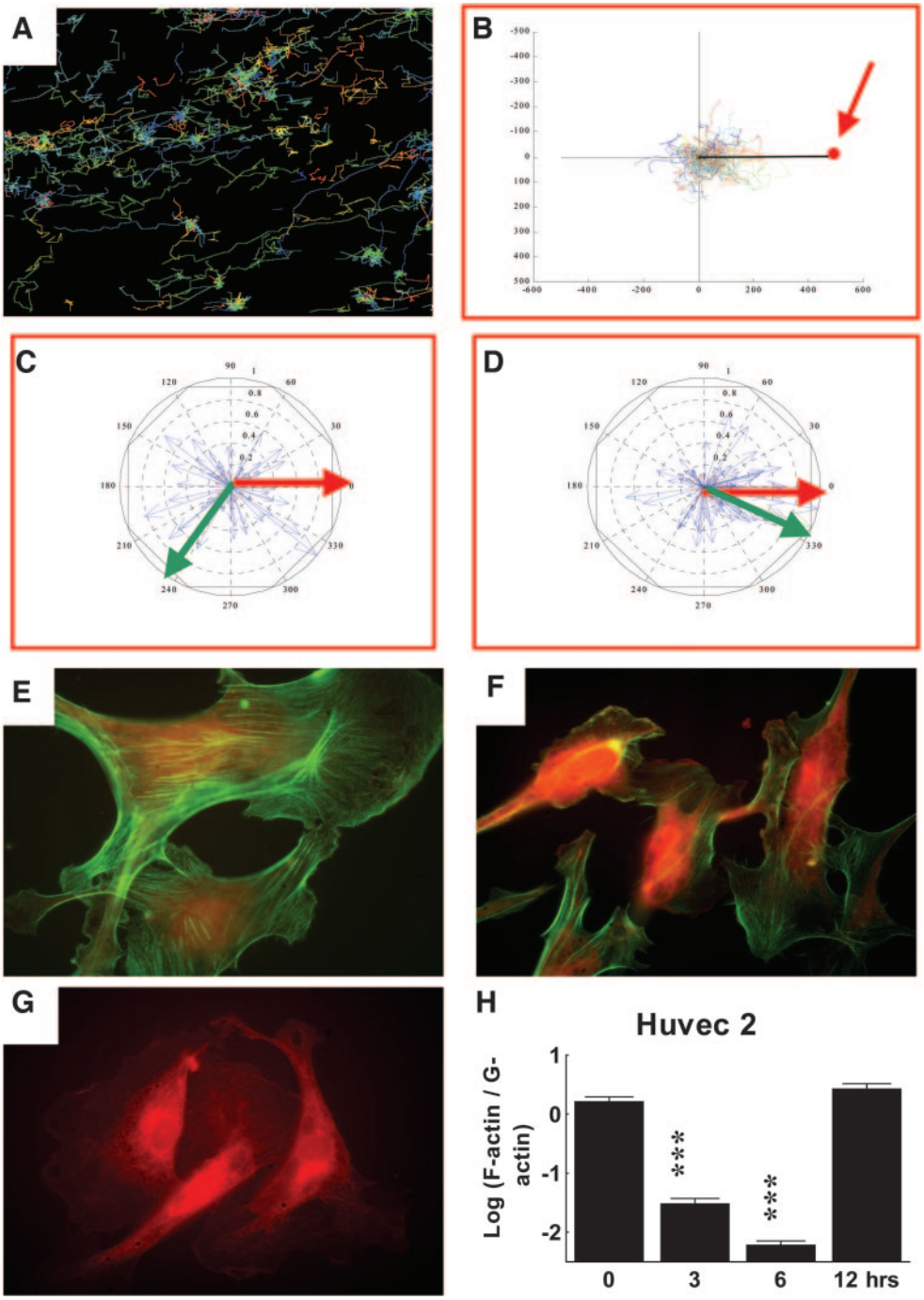

Fig. 6 G17-induced chemotactic effects on HUVEC migration and actin cytoskeleton organization. *A*, illustration of the individual trajectories traveled by HUVECs on gelatin during an 8-hour period of observation by means of computer-assisted videomicroscopy. In *B*, all of the initial cell positions are set to the origin (0,0) of the axes. The gradient direction is arbitrarily fixed in an easterly direction (the *red dot* highlighted by the *red arrow*). The *red arrows* in *C* and *D* thus indicate the point where either saline (control) or 10 nmol/L G17 was added. Each individual HUVEC trajectory is characterized by means of its αMRDO vector (joining the initial and most distant cell positions) in *C* and *D* (*blue arrows*). These figures also compare the resulting direction of all of the αMRDO vectors (*green arrows*) with the gradient direction (*red arrows*). *E*−*G*, morphologic appearance of the fibrillary (*green fluorescence*) as opposed to the globular (*red fluorescence*) actin in the cytoskeletons of untreated HUVECs (*E*) or of HUVECs treated for 3 (*F*) or 6 hours (*G*) with 10 nmol/L G17. The ratio of fibrillary/globular actin was quantitatively determined by means of computer-assisted fluorescence microscopy (*H*).

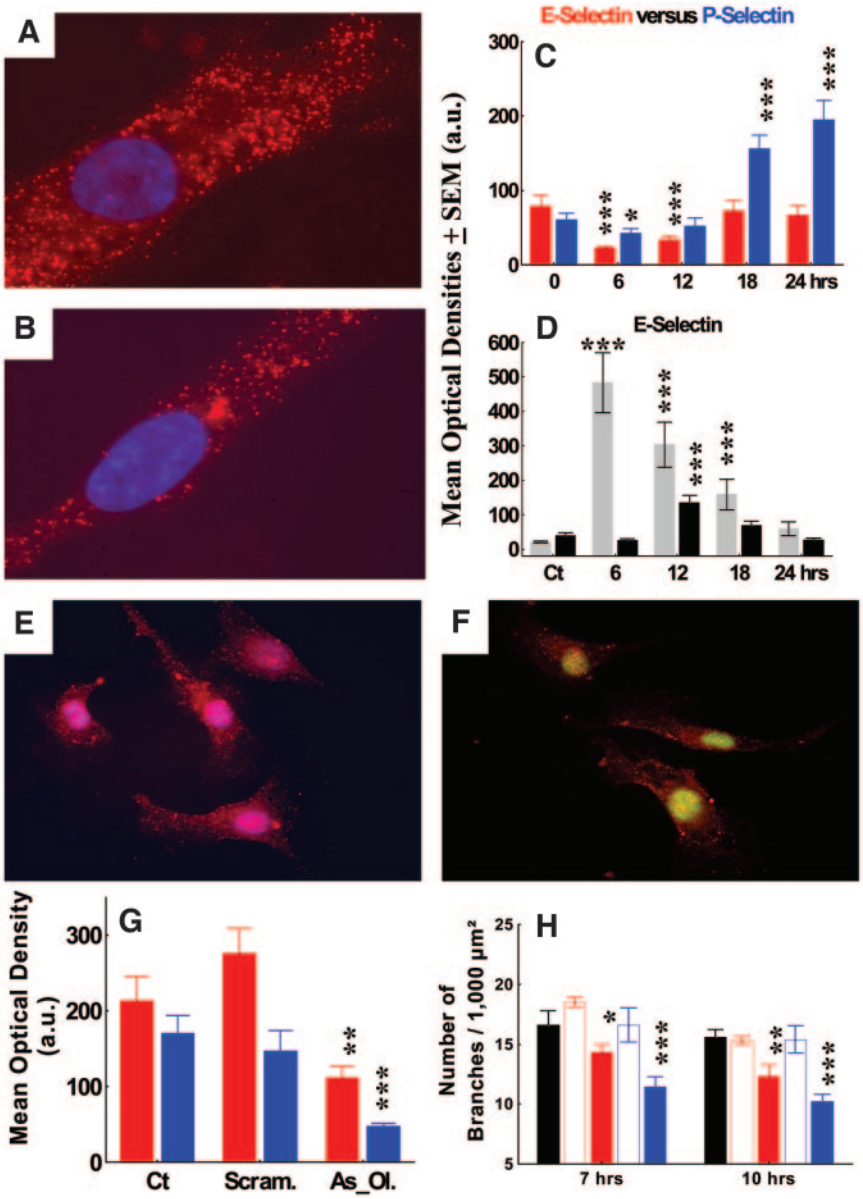

Fig. 7 G17–, IL-8–, and IL-1β–induced effects on E- and P-selectin expression in HUVECs (Huvec 1). *A* and *B*, immunofluorescence patterns of E-selectin expression (*red*) in an untreated HUVEC or in a HUVEC treated for 6 hours with 10 nmol/L G17. *C*, as revealed by quantitative immunofluorescence, the influence for HUVECs of 10 nmol/L G17 (for 6–24 hours) on E-selectin (*red bars*) and P-selectin (*blue bars*) expression. *D*, influence of 1 nmol/L IL-1β (▒) and 1 nmol/L IL-8 (■) after various incubation times for HUVECs (6–24 hours) on E-selectin expression revealed by quantitative immunofluorescence. *E* and *F*, morphologic illustration of E-selectin expression (revealed by means of red fluorescence immunocytochemistry) in untreated HUVECs (*E*) or HUVECs incubated for 6 hours in the presence of 0.01 μmol/L E-selectin green fluorescent antisense oligonucleotides (*F*). *G*, quantitative determination (by means of computer-assisted fluorescence microscopy) of E-selectin (*red bars*) and P-selectin (*blue bars*) expression in the absence (control, *Ct*) and the presence for 6 hours of 0.01 μmol/L scrambled (*Scram.*) or 0.01 μmol/L antisense (*As_Ol.*) E- and P-selectin oligonucleotides. Between 50 and 100 HUVECs were analyzed in each experimental condition. *H*, characterization of the influence of 0.01 μmol/L scrambled (*red open bars*) E-selectin, 0.01 μmol/L antisense E-selectin (*red bars*), 0.01 μmol/L scrambled P-selectin (*blue open bars*), and 0.01 μmol/L antisense P-selectin (*blue bars*) oligonucleotides (as compared with control, *i.e.*, without oligonucleotides; ■) on the ability of HUVECs to form capillary networks 7 and 10 hours after their *in vitro* seeding on Matrigel (see Fig. 3). The data are presented as means (*bars*) ± SE (*thin bars*), with * = $P < 0.05$, ** = $P < 0.01$, and *** = $P < 0.001$ (as compared with control).

then quantitatively determined (by means of computer-assisted fluorescent microscopy) the levels of E- or P-selectin in the transfected (*red* and *green* = *yellow*) HUVECs (Fig. 7*F*). Fig. 7G illustrates the E-selectin (*red bars*) and P-selectin (*blue bars*) expression in untreated HUVECs (*Ct*) or in HUVECs transfected with a scrambled oligonucleotide (*Scram.*) or an actual antisense oligonucleotide (*As_Ol.*). Fig. 7*G* shows that a concentration of 0.01 μmol/L E (*red bars*)- or P-selectin anti-

sense oligonucleotides (*blue bars*) was able to decrease the levels of E- or P-selectin membrane expression in the HUVECs both selectively (as compared with scrambled oligonucleotides) and significantly. As illustrated in Fig. 7*H*, the use of this concentration of E (*red bars*)- and P-selectin antisense oligonucleotides (*blue bars*) significantly decreased the ability of the HUVECs to form capillary-like structures, as compared with control (absence of oligonucleotides; ■) and with conditions involving scrambled oligonucleotides for E- (*open red bars*)- and P-selectins (*open blue bars*).

DISCUSSION

Angiogenesis, tumor cell proliferation, and migration are the hallmarks of all malignant tumors in general and of malignant gliomas in particular. We have already shown the roles played by gastrin in glioma cell proliferation (12–14) and migration (13, 15–17). We show here that gastrin is also able to induce proangiogenic effects both *in vivo* in experimental U373 orthotopic xenografts and *in vitro* in HUVECs. The presence of mRNAs in the case of CCK_A, CCK_B, and CCK_C receptors was evidenced by means of RT-PCR (whose products were sequenced) in three independent HUVEC primocultures as well as in microvessels dissected from a human glioblastoma. The fact that the GBM microvessels expressed the three types of gastrin receptors in the same way as the HUVECs partly validated the use of the HUVECs as an experimental model to characterize G17-induced effects in the case of angiogenesis in experimental gliomas. However, the fact remains that neoangiogenesis in gliomas is related to microvessels, whereas HUVECs originate from large vessels.

Whereas G17 increased neoangiogenesis in orthotopic xenografts of U373 human gliomas, CCK had marginal effects only (see Fig. 1), and this is the reason why we decided to remain focused on G17-mediated effects on angiogenesis alone. A CCK_B receptor antagonist (L365,260) significantly antagonized the *in vivo* G17-mediated proangiogenic effects in the U373 gliomas, whereas a CCK_A receptor antagonist (L364,718) did not. In the same way, whereas daily delivery of L365,260 over several weeks to orthotopic U373 glioma-bearing nude mice significantly increased their survival periods as compared with control mice, L364,718 did not induce any such therapeutic benefit. The G17-induced increase in the survival periods of the U373 glioma-bearing nude mice was paralleled by a significant G17-induced decrease in neoangiogenesis in these gliomas. All these data therefore strongly suggest that, *in vivo*, G17 has a proangiogenic effect on malignant experimental gliomas, an effect that could be (at least partly) mediated by the CCK_B receptor. We also observed that G17 induced large lacunae full of blood, as illustrated in Fig. 1*G*. This process could correspond to a marked G17-mediated proangiogeneic effect leading to endothelial cell sprouting, but with incomplete vessel formation, a feature that is commonly observed in tumor neoangiogenesis (58).

We also observed that the daily administration of L365,260 to nude mice bearing orthotopic xenografts of human BxPC-3 pancreas cancer cells significantly decreased neoangiogenesis levels in these xenografts (data not shown). In the same manner, we observed that the daily administration of both L365,260 and L364,718 to nude mice bearing subcutaneous xenografts of human C32 melanoma cells significantly decreased angiogenesis in these xenografts, with a concomitant decrease in the growth rates of these experimental melanomas.[8]

The *in vitro* data obtained on the HUVECs indicate that G17 speeds up the HUVEC-related tubulogenesis process during the first hours of HUVEC culture on Matrigel, but without modifying the subsequent pattern of HUVEC tubulogenesis. These effects seem to be largely dependent on the CCK_B receptor (see Fig. 3*F*). The fact that the concomitant administration of L365,260 and L364,718 induced slightly, but nevertheless significantly, more marked antagonistic effects against G17-induced proangiogenic influences than L365,260 alone could relate to heterodimerization processes between CCK_B and CCK_A receptors (31).

The G17-mediated acceleration of HUVEC tubulogenesis seems to be partly mediated by PI3K because a PI3K antagonist (LY294,002) was able to significantly antagonize the G17-mediated proangiogenic effects on HUVEC tubulogenesis (see Fig. 4*A*). In contrast, PKC seems to be less involved in G17-mediated effects on HUVEC tubulogenesis because the PKC inhibitor Ro320,432 did not antagonize the G17-induced proangiogenic effects on HUVEC tubulogenesis (Fig. 4*D*). Pagliocca *et al.* (46) observe that when AGS gastric cancer cells (which are CCK_B receptor positive) are cultured on plastic, gastrin stimulates cell adhesion, the formation of lamellipodia, and the extension of the already long processes in part by the activation of PKC and PI3K as observed here. Branching morphogenesis was not observed in these circumstances (46), as in the case of the gelatin-cultured HUVECs. When AGS cells were cultured on an artificial basement membrane, the same stimuli increased the formation of organized multicellular arrays exhibiting branching morphogenesis (46). These effects were reversed by PKC inhibitors, but not by PI3K inhibitors (46). In our study, we observed the reverse features in the case of the HUVECs, a fact that could relate to different intracellular signaling pathways activated by gastrin in gastric cancer cells as compared with normal endothelial cells. We observed slight, but nevertheless significant, modifications induced by gastrin at the levels of expression of both PKCα and PKCμ (data not shown). These two PKC isoforms are involved in gastrin-mediated modifications of the actin cytoskeleton (59, 60).

G17 stimulates the activities of various genes (including IL-8 and E-selectin) via activation of the NF-κB pathway (43), and the levels of activation of the NF-κB pathway play important roles in survival processes of endothelial cells against cytotoxic influences (48). Three of the four regulatory elements found in the human E-selectin promoter are NF-κB binding sites (49).

NF-κB is a collective designation for a family of highly regulated dimer transcription factors (61). Virtually all vertebrate cells express at least one of five Rel/NF-κB members, namely, p50/p105 (NF-κB1), p52/100 (NF-κB2), c-Rel, p65 (RelA), and RelB, which are assembled into homo- and het-

[8] V. Mathieu, T. Mijatovic, and R. Kiss. Gastrin decreases human melanoma cell invasiveness in association with modifications both to the levels of expression of MT1-MMP (MMP-14), the plasminogen activator inhibitor-2 (PAI-2) and the alphaVbeta3 integrin, and to the organization of the actin cytoskeleton, manuscript in preparation.

erodimers (ref. 62; Fig. 5*C*). Almost every kinase pathway explored was found to participate in NF-κB activation [examples include PKC, Akt/protein kinase B, c-Jun-NH_2-terminal kinase, mitogen-activated protein kinase kinase kinase, and mitogen-activated protein/kinase/ERG kinase kinase (Fig. 5*C*)], but few have been corroborated by genetic data (63). With few exceptions (*e.g.,* H_2O_2 and UV radiation), all of the signals converge to activate IκB kinase, leading to IκB phosphorylation, ubiquitination, and degradation, a process that enables the nuclear translocation of NF-κB dimers and their binding to DNA (ref. 64; Fig. 5*C*). Once activated, IKK phosphorylates the bulk of the cytoplasmic IκB pool, promoting its degradation and NF-κB activation (ref. 64; Fig. 5*C*). IκB represents a family of NF-κB inhibitors, of which IκBα, IκBβ, and IκBε are the chief regulators in mammalians (ref. 64; Fig. 5*C*). We made use of three NF-κB inhibitors, *i.e.,* Parthenolide, BAY-11-7085, and CAPE (see Fig. 5*C*), and we observed that these inhibitors exerted no effects or only weak antagonistic effects against G17-mediated proangiogenic effects with respect to the HUVEC tubulogenesis process (see Fig. 5*D*). These data fit in with those illustrated in Fig. 5*B*, which shows that G17 did not activate NF-κB DNA binding activity in HUVECs during the first 2 hours after the addition of G17 to the HUVEC culture media.

The use of a cDNA microarray approach showed that, like GBM microvessels, HUVECs express mRNAs for both TNF-α and IL-8, two major regulators of angiogenesis (9–11). We observed that G17 markedly stimulates IL-8 release by HUVECs. However, the G17-induced increase in IL-8 release by the HUVECs (Fig. 5*A*) occurred after the G17-induced proangiogenic effects on HUVEC tubulogenesis (Fig. 3*E*), a fact that strongly suggests that this G17-induced proangiogenic effect is IL-8 independent. In the same way, whereas G17 induced chemotactic effects on individual HUVECs, IL-8 did not. The absence of IL-8–mediated chemotactic effects on the HUVECs can be at least partly explained by the absence of CXCR1 (IL-8 receptor α) and CXCR2 (IL-8 receptor β) in the HUVEC primocultures that we used. The presence of CXCR1 and CXCR2 receptors varies largely among different HUVEC primocultures and among different *in vitro* models of microvessels (39–41, 44).

One of the major classes of adhesion molecules present on the surface of endothelial cells includes selectins (49). The direct implication of P-selectin (but not E-selectin, at least to our knowledge) in endothelial cell migration has been reported previously (50). The present data show that G17 transiently decreased the levels of expression of E-selectin in the HUVECs during the first 12 hours after G17 addition to the culture medium (see Fig. 7*C*). These G17-induced effects on E-selectin could also relate to an activation of the E-selectin internalization processes mediated by gastrin, a process which could render HUVECs less adhesive to the basement membrane (Matrigel) and therefore help in their tubulogenesis-related migratory processes. The present study suggests a direct implication of E-selectin in HUVEC migration during the tubulogenesis process.

In conclusion, the present data show that gastrin induces marked proangiogenic effects both *in vitro* and *in vivo* (in experimental glioma), a process that seems to be IL-8 independent but could, at least in part, depend on the level of E-selectin activation.

ACKNOWLEDGMENTS

We thank ML Laboratories PLC (London, UK) for providing the L365,260 and L364,718 compounds.

REFERENCES

1. Bacher M, Schrader J, Thompson N, et al. Up-regulation of macrophage migration inhibitory factor gene and protein expression in glial tumor cells during hypoxic and hypoglycemic stress indicates a critical role for angiogenesis in glioblastoma multiforme. Am J Pathol 2003; 162:11–7.

2. Kleihues P, Cavenee WK. Pathology and genetics of tumours of the nervous system, 2nd Edition, International Agency for Research on Cancer and WHO Health Organisation. Oxford, United Kingdom: Oxford Press; 2000.

3. Brat DJ, Castellano-Sanchez A, Kaur B, Van Meir EG. Genetic and biologic progression in astrocytomas and their relation to angiogenic dysregulation. Adv Anat Pathol 2002;9:24–36.

4. Griscelli F, Li H, Cheong C, et al. Combined effects of radiotherapy and angiostatin gene therapy in glioma tumor model. Proc Natl Acad Sci USA 2000;97:6698–703.

5. Kunkel P, Ulbricht U, Bohlen P, et al. Inhibition of glioma angiogenesis and growth in vivo by systemic treatment with a monoclonal antibody against vascular endothelial growth factor receptor-2. Cancer Res 2001;61:6624–8.

6. Bello L, Lucini V, Costa F, et al. Combinatorial administration of molecules that simultaneously inhibit angiogenesis and invasion leads to increased therapeutic efficacy in mouse models of malignant glioma. Clin Cancer Res 2004;10:4527–37.

7. Schmidt NO, Ziu M, Carrabba G, et al. Antiangiogenic therapy by local intracerebral microinfusion improves treatment efficiency and survival in an orthotopic human glioblastomas model. Clin Cancer Res 2004;10:1255–62.

8. Gondi CS, Lakka SS, Yanamandra N, et al. Adenovirus-mediated expression of antisense urokinase plasminogen activator receptor and antisense cathepsin B inhibits tumor growth, invasion, and angiogenesis in gliomas. Cancer Res 2004;64:4069–77.

9. Zetter BR. Angiogenesis and tumor metastasis. Annu Rev Med 1998;49:407–24.

10. Diestler O, Neidhart M, Gay RE, Gay S. The molecular control of angiogenesis Intern Rev Immunol 2002;21:33–49.

11. Folkman J, D'Amore PA. Blood vessel formation: What is its molecular basis? Cell 1996;87:1153–5.

12. Camby I, Salmon I, Danguy A, et al. Influence of gastrin on human astrocytic tumor cell proliferation. J Natl Cancer Inst 1996;88:594–600.

13. De Hauwer C, Camby I, Darro F, et al. Gastrin inhibits motility, decreases cell death levels and increases proliferation in human glioblastoma cell lines. J Neurobiol 1998;37:373–82.

14. Lefranc F, Sadeghi N, Metens T, et al. Characterization of gastrin-induced cytostatic effect on cell proliferation in experimental gliomas. Neurosurgery 2003;52:881–91.

15. Kucharczak J, Pannequin J, Camby I, et al. Gastrin induces overexpression of genes involved in human U373 glioblastoma cell migration. Oncogene 2001;20:7021–8.

16. Pannequin J, Oiry C, Morel C, et al. C-terminal heptapeptide of gastrin inhibits astrocytomas cell motility by interacting with a new gastrin binding site. J Pharmacol Exp Ther 2002;302:274–82.

17. Lefranc F, Camby I, Belot N, et al. Gastrin significantly modifies the migratory abilities of experimental glioma cells. Lab Investig 2002; 82:1241–52.

18. Saal I, Gustin A, Rombaut K, et al. Laser-assisted microdissection applied to frozen surgical pathological specimens: methodological aspects on RT-PCR. J Exp Ther Oncol 2003;3:325–35.

19. Larsson LI, Rehfeld JF. Localization and molecular heterogeneity of cholecystokinin in the central and peripheral nervous system. Brain Res 1979;165:201–18.

20. Innis RB, Correa FM, Uhl GR, Schneider B, Snyder SH. Cholecystokinin octapeptide-like immunoreactivity: histochemical localization in rat brain. Proc Natl Acad Sci USA 1979;76:521–5.

21. Rehfeld JF, Kruse-Larsen C. Gastrin and cholecystokinin in human cerebrospinal fluid. Immunochemical determination of concentrations and molecular heterogeneity. Brain Res 1978;155:19–26.

22. Vanderhaeghen JJ, Signeau JC, Gepts W. New peptide in the vertebrate CNS reacting with antigastrin antibodies. Nature (Lond) 1975;257:604–5.

23. Robberecht P, Deschodt-Lanckman M, Vanderhaeghen JJ. Demonstration of biological activity of brain gastrin-like peptidic material in the human: its relationship with the COOH-terminal octapeptide of cholecystokinin. Proc Natl Acad Sci USA 1978;75:524–8.

24. Rehfeld JF, Van Solinge WW. The tumor biology of gastrin and cholecystokinin. Adv Cancer Res 1991;63:295–347.

25. Rehfeld JF. How to measure cholecystokinin in tissue, plasma and cerebrospinal fluid. Regul Pept 1998;78:31–9.

26. Heasley LE. Autocrine and paracrine signaling through neuropeptide receptors in human cancer. Oncogene 2001;20:1563–9.

27. Aly A, Shulkes A, Baldwin GS. Gastrins, cholecystokinins and gastrointestinal cancer. Biochim Biophys Acta 2004;1704:1–10.

28. Iwata N, Murayama T, Matsumori Y, et al. Autocrine loop through cholecystokinin-B/gastrin receptors involved in growth of human leukemia cells. Blood 1996;88:2683–9.

29. Schaer JC, Reubi JC. High gastrin and cholecystokinin (CCK) gene expression in human neuronal, renal, and myogenic stem cell tumors: comparison with CCK-A and CCK-B receptor contents. J Clin Endocr Metab 1999;84:233–9.

30. Wank SA. Cholecystokinin receptors. Am J Physiol Gastrointest Liver Physiol 1995;269:G628–46.

31. Cheng ZJ, Harikumar KG, Holicky EL, Miller LJ. Heterodimerization of type A and B cholecystokinin receptors enhance signaling and promote cell growth. J Biol Chem 2003;278:52972–9.

32. Baldwin GS, Chandler R, Scanlon DB, Weinstock J. Identification of a gastrin binding protein in porcine gastric mucosal membranes by covalent cross-linking with iodinated gastrin. J Biol Chem 1986;261:12252–7.

33. Reubi JC, Schaer JC, Waser B. Cholecystokinin (CCK)-A and CCK-B/gastrin receptors in human tumors. Cancer Res 1997;57:1377–86.

34. Lefranc F, Chaboteaux C, Belot N, et al. Determination of RNA expression for cholecystokinin/gastrin receptors (CCK_A, CCK_B and CCK_C) in human tumors of the central and peripheral nervous system. Int J Oncol 2003;22:213–9.

35. Smith JP, Verderame MF, McLaughlin P, et al. Characterization of the CCK-C (cancer) receptor in human pancreatic cancer. Int J Mol Med 2002;10:689–94.

36. Seva C, Dickinson CJ, Yamada T. Growth promoting effects of glycine-extended progastrin. Science (Wash DC) 1994;265:410–2.

37. Singh P, Owlia A, Espeijo R, et al. Novel gastrin receptors mediate mitogenic effects of gastrin and processing intermediates of gastrin on Swiss 3T3 fibroblasts. Absence of detectable cholecystokinin (CCK)-A and CCK-B receptors. J Biol Chem 1995;270:8429–38.

38. Rehfeld JF, Larsson LI, Gottermann NR, et al. Neural regulation of pancreatic hormone secretion by the C-terminal tetrapeptide of CCK. Nature (Lond) 1980;284:33–8.

39. Salcedo R, Resau JH, Halverson D, et al. Differential expression and responsiveness of chemokine receptors (CXCR1–3) by human microvascular endothelial cells and umbilical vein endothelial cells. FASEB J 2000;14:2055–64.

40. Schraufstatter IU, Trieu K, Zhao M, et al. IL-8-mediated cell migration in endothelial cells depends on cathepsin B activity and transactivation of the epidermal growth factor receptor. J Immunol 2003;171:6714–22.

41. Li A, Dubey S, Varney ML, Dave BJ, Singh RK. IL-8 directly enhanced endothelial cell survival, proliferation, and matrix metalloproteinases production and regulated angiogenesis. J Immunol 2003;170:3369–76.

42. Oynebraten I, Bakke O, Brandtzaeg P, Johansen FE, Haraldsen G. Rapid chemokine secretion from endothelial cells originates from 2 distinct compartments. Blood 2004;104:314–20.

43. Hiraoka S, Miyazaki Y, Kitamura S, et al. Gastrin induces CXC chemokine expression in gastric epithelial cells through activation of NF-kappaB. Am J Physiol Gastrointest Liver Physiol 2001;281:G735–42.

44. Heidemann J, Ogawa H, Dwinell MB, et al. Angiogenic effects of interleukin-8 (CXCL8) in human intestinal microvascular endothelial cells are mediated by CXCR2. J Biol Chem 2003;278:8508–15.

45. Renard P, Ernest I, Houbion A, et al. Development of a sensitive multi-well colorimetric assay for active NF-kappaB. Nucleic Acids Res 2001;29:1–5.

46. Pagliocca A, Wroblewski LE, Ashcroft FJ, et al. Stimulation of the gastrin-cholecystokinin B receptor promotes branching morphogenesis in gastric AGS cells. Am J Physiol Gastrointest Liver Physiol 2002;283:G292–9.

47. Debeir O, Camby I, Kiss R, Van Ham P, Decaestecker C. A model-based approach for automated in vitro cell tracking and chemotaxis analyses. Cytometry 2004;60A:29–40.

48. Zen K, Karsan A, Stempien-Otero A, et al. NF-kappaB activation is required for human endothelial survival during exposure to tumor necrosis factor-alpha but not to interleukin-1beta or lipopolysaccharide. J Biol Chem 1999;274:28808–15.

49. Vestweber D, Blanks JE. Mechanisms that regulate the function of the selectins and their ligands. Physiol Rev 1999;79:181–213.

50. Morbidelli L, Brogelli L, Crancer HJ, Ziche M. Endothelial cell migration is induced by soluble P-selectin. Life Sci 1998;62:7–11.

51. Branle F, Lefranc F, Camby I, et al. Evaluation of the efficiency of chemotherapy in in vivo orthotopic models of human glioma cells with and without 1p19q deletions and in C6 rat orthotopic allografts serving for the evaluation of surgery combined with chemotherapy. Cancer (Phila) 2002;95:641–55.

52. Belot N, Rorive S, Doyen I, et al. The molecular characterization of cell-substratum attachments in human glial tumors relates to prognostic features. Glia 2001;36:375–90.

53. Farinelle S, DeHauwer C, Darro F, et al. Setting up of an original computer-assisted methodology to characterize in vitro drug-induced anti-angiogenic effects. Int J Mol Med 1998;2:545–53.

54. Gimbrone MA, Cotran RS, Folkman J. Human vascular endothelial cells in culture: growth and DNA synthesis. J Cell Biol 1974;60:673–84.

55. Rosner B. Fundamentals of Biostatistics. London: International Thomson Publishing; 1995.

56. Siegel S, Castellan NJ Jr. Nonparametric Statistics for the Behavioral Sciences, 2nd ed. Singapore: McGraw-Hill; 1988.

57. Mardia KV. Directional statistics, 2nd ed. New York: Wiley; 1999.

58. Baluk P, Morikawa S, Haskell A, Mancuso M, McDonald DM. Abnormalities of basement membrane on blood vessels and endothelial sprouts in tumors. Am J Pathol 2003;163:1801–15.

59. Williams JA. Intracellular signaling mechanisms activated by cholecystokinin-regulating synthesis and secretion of digestive enzymes in pancreatic acinar cells. Annu Rev Physiol 2001;63:77–97.

60. Rozengurt E, Walsh JH. Gastrin, CCK, signaling and cancer. Annu Rev Physiol 2001;63:49–76.

61. Amit S, Ben-Neriah Y. NF-kappaB activation in cancer: a challenge for ubiquitination- and proteasome-based therapeutic approach. Semin Cancer Biol 2003;13:15–28.

62. Ghosh S, May MJ, Kopp EB. NF-kappaB and Rel proteins: evolutionarily conserved mediators of immune response. Annu Rev Immunol 1998;16:225–60.

63. Karin M, Ben-Neriah Y. Phosphorylation meets ubiquitination: the control of NF-kappaB activity. Annu Rev Immunol 2000;18:621–63.

64. Whiteside ST, Israel A. I kappa B protein: structure, function and regulation. Semin Cancer Biol 1997;8:75–82.